PB87-115747

Curvilinear Finite Element Model for Simulating Two-Well Tracer Tests and Transport in Stratified Aquifers

GeoTrans, Inc., Herndon, VA

Prepared for

Robert S. Kerr Environmental Research Lab.
Ada, OK

1986

U.S. Department of Commerce
National Technical Information Service
NTIS

PB87-115747

TECHNICAL REPORT DATA
(Please read Instructions on the reverse before completing)

1. REPORT NO.	2.	3. RECIPIENT'S ACCESSION NO.
EPA/600/J-86/146		

4. TITLE AND SUBTITLE
A CURVILINEAR FINITE ELEMENT MODEL FOR SIMULATING TWO-WELL TRACER TESTS AND TRANSPORT IN STRATIFIED AQUIFERS (Journal Version)

5. REPORT DATE
1986

6. PERFORMING ORGANIZATION CODE

7. AUTHOR(S)
Peter S. Huyakorn[a], Peter F. Andersen[a], Oktay Guven[b], and Fred J. Molz[b]

8. PERFORMING ORGANIZATION REPORT NO.

9. PERFORMING ORGANIZATION NAME AND ADDRESS
[a]GeoTrans, Inc., Herndon, VA 22070

[b]Dept. of Civil Engineering
Auburn University, AL 36849

10. PROGRAM ELEMENT NO.
ABPC1A

11. CONTRACT/GRANT NO.
CR-810704-01-0

12. SPONSORING AGENCY NAME AND ADDRESS
U.S. Environmental Protection Agency
Robert S. Kerr Environmental Research Laboratory
P.O. Box 1198
Ada, OK 74820

13. TYPE OF REPORT AND PERIOD COVERED

14. SPONSORING AGENCY CODE
EPA-600/15

15. SUPPLEMENTARY NOTES
Project Officer: Lowell E. Leach, FTS 743-2333
Water Resources Research, 22(5):663-678, May 1986

16. ABSTRACT

The problem of solute transport in steady nonuniform flow created by a recharging and discharging well pair is investigated. Numerical difficulties encountered with the standard Galerkin formulations in Cartesian coordinates are illustrated. An improved finite element solution strategy is presented to overcome the numerical problem. The strategy is based on a formulation performed in three-dimensional curvilinear coordinates. This formulation is developed especially for the simulation of two-well injection-withdrawal tracer tests conducted in homogeneous or stratified aquifers. The formulation can also be applied to other types of problems involving transport in homogeneous and stratified aquifers. A three-dimensional finite element approximation is derived by two successive applications of upstream weighted-residual and subdomain collocation procedures.

17. KEY WORDS AND DOCUMENT ANALYSIS

a. DESCRIPTORS	b. IDENTIFIERS/OPEN ENDED TERMS	c. COSATI Field/Group

18. DISTRIBUTION STATEMENT	19. SECURITY CLASS *(This Report)*	21. NO. OF PAGES
RELEASE TO PUBLIC	UNCLASSIFIED	17
	20. SECURITY CLASS *(This page)*	22. PRICE
	UNCLASSIFIED	

EPA Form 2220-1 (Rev. 4-77) PREVIOUS EDITION IS OBSOLETE

REPRODUCED BY
U.S. DEPARTMENT OF COMMERCE
NATIONAL TECHNICAL
INFORMATION SERVICE
SPRINGFIELD, VA 22161

WATER RESOURCES RESEARCH, VOL. 22, NO. 5, PAGES 663–678, MAY 1986

EPA/600/J-86/146
JOURNAL ARTICLE

A Curvilinear Finite Element Model for Simulating Two-Well Tracer Tests and Transport in Stratified Aquifers

PETER S. HUYAKORN AND PETER F. ANDERSEN

GeoTrans, Inc., Herndon, Virginia

OKTAY GÜVEN AND FRED J. MOLZ

Department of Civil Engineering, Auburn University, Auburn, Alabama

The problem of solute transport in steady nonuniform flow created by a recharging and discharging well pair is investigated. Numerical difficulties encountered with the standard Galerkin formulation in Cartesian coordinates are illustrated. An improved finite element solution strategy is presented to overcome the numerical problem. The strategy is based on a formulation performed in three-dimensional curvilinear coordinates. This formulation is developed especially for the simulation of two-well injection-withdrawal tracer tests conducted in homogeneous or stratified aquifers. The formulation can also be applied to other types of problems involving transport in homogeneous and stratified aquifers. A three-dimensional finite element approximation is derived by two successive applications of upstream weighted-residual and subdomain collocation procedures. First, the weighted residual procedure is formulated in the horizontal flow plane using curvilinear coordinates along and normal to streamlines. Upstream weighting is included but automatically controlled and limited to one dimension along the main flow direction. Second, the subdomain collocation procedure is formulated in the vertical dimension. Spatial discretization of the three-dimensional flow region is performed using a curvilinear finite element mesh that is point-centered in the horizontal plane and block-centered in the vertical direction. General algorithms are developed for mesh generation, time stepping and matrix reduction. The solution algorithm is designed to accommodate several thousand nodal unknowns with minimal core storage and CPU time requirement. Two simulation examples are presented to verify and validate the numerical model in two dimensions using an analytical solution and experimental laboratory and field data. A comparative study shows that the proposed formulation is superior to the standard Galerkin formulation in Cartesian coordinates both in terms of accuracy and computational efficiency. The field simulation example indicates the need to conduct a more elaborate three-dimensional simulation study allowing for vertical variation in hydraulic conductivity. Such a study has been completed and is reported in the follow-up paper of this series.

INTRODUCTION

Studies pertaining to analysis and prediction of solute transport between a recharging and discharging well pair have received considerable attention for two decades. These studies are important from several practical standpoints. Typical examples include (1) the risk assessment of liquid waste injection in aquifers that are used for water supply, and (2) the design and analysis of two-well injection-withdrawal tracer tests. Traditionally, analytical solutions have been used for predicting concentration distributions and the rate of plume migration. For two-well tracer test simulations, there are several analytical solutions available. Among these are the solutions presented by *Hoopes and Harleman* [1967*a*], *Gelhar* [1982], and *Grove and Beetem* [1971]. All of these solutions are based on simplified assumptions of isotropic and homogeneous confined aquifers and negligible dispersion across the streamlines. Despite these limitations, the analytical models have been successfully applied to laboratory and field experimental data [see *Hoopes and Harleman*, 1967*a*; *Webster et al.*, 1970; and *Grove and Beetem*, 1971; *Grove*, 1971; and *Claasen and Cordes*, 1975].

Numerical techniques provide an alternative tool for simulating two-well tracer tests. In terms of flexibility and ability to deal with more complex field conditions and account for combined influences of longitudinal and lateral hydrodynamic dispersion and advection, the numerical models offer significant advantages over the analytical solutions. However, difficulties are often encountered with available numerical (finite difference and finite element) models when one attempts to simulate cases where dispersivity values are two or three orders of magnitude less than well spacings. For such cases, the numerical solutions obtained often exhibit unacceptable oscillations and excessive artificial dispersion unless the grid chosen is very refined. Unfortunately, the computational cost resulting from the use of such a grid can be excessive, particularly if the simulation is performed in three dimensions.

To overcome the numerical problem, we present an improved finite element formulation performed in the three-dimensional curvilinear coordinates. This formulation is developed especially for the simulation of two-well injection-withdrawal tracer tests conducted in homogeneous and layered aquifers. Included in this formulation is the solution technique designed to provide cost-effective and reliable simulations of difficult cases where longitudinal dispersivity to well spacing ratios are too small to be accommodated by the standard Galerkin formulation in Cartesian coordinates. The numerical procedures to be described contain several other salient features including (1) automatically controlled upstream weighting along streamlines, (2) efficient time stepping and matrix handling schemes, and (3) schemes for generating an optimal curvilinear flow net.

Copyright 1986 by the American Geophysical Union.

Paper Number 5W4126.
0043-1397/86/005W-4126

NTIS is authorized to reproduce and sell this report. Permission for further reproduction must be obtained from the copyright owner.

TABLE 1. Values of Physical Parameters and Discretization Data Used to Simulate the Laboratory Tracer Test by Hoopes and Harleman

Parameter	Value
Well flow rate, Q	2.339 cm^3/s
Well spacing, $2x_0$	61.0 cm
Thickness of aquifer model, b	8.9 cm
Porosity, ϕ	0.374
Lateral dispersivity, α_T	0.
Case 1, longitudinal dispersivity, α_L	2.94 cm
Case 2, longitudinal dispersivity, α_L	0.294 cm
x_i (cm), $i = 1, 2, \cdots, 29$	−145., −120., −100., −80., −60., −50., −40., −35., −30.5, −25., −20., −15., −10., −5., 0., 5., 10., 15., 20., 25., 30.5, 35., 40., 50., 60., 80., 100., 120., 145
y_j (cm), $j = 1, 2, \cdots, 15$	0., 5., 10., 15., 20., 25., 30., 35., 40., 50., 60., 80., 100., 120., 145
$\Delta t_1 = 50$ s, $\Delta t_k = 1.2\ \Delta t_{k-1} \leq 300$ s for $k = 2, \cdots, 50$	

Data from *Hoopes and Harleman* [1967*a*].

The present paper deals with the development and application of a curvilinear finite element model for simulating two-well tracer tests. The overall objective is to provide an efficient, accurate and stable numerical basis for analyzing two-well tracer tests and predicting contaminant transport in homogeneous and locally stratified aquifers.

Statement of Transport Problem and Numerical Difficulties

To illustrate numerical difficulties encountered with the standard Galerkin formulation, we consider a simple situation of two-dimensional transport of a conservative solute between a pair of recharging and discharging wells fully penetrating a homogeneous and isotropic aquifer and operating at a constant flow rate. This situation may be described using the following form of the advective-dispersive equation [*Bear*, 1979]:

$$\frac{\partial}{\partial x}\left(D_{xx}\frac{\partial c}{\partial x}\right)+\frac{\partial}{\partial y}\left(D_{yy}\frac{\partial c}{\partial y}\right)+\frac{\partial}{\partial x}\left(D_{xy}\frac{\partial c}{\partial y}\right)+\frac{\partial}{\partial y}\left(D_{yx}\frac{\partial c}{\partial x}\right)-\frac{V_x}{\theta}\frac{\partial c}{\partial x}-\frac{V_y}{\theta}\frac{\partial c}{\partial y}=\frac{\partial c}{\partial t} \quad (1)$$

where c is the solute concentration, V_x and V_y are Darcy velocity components along the x and y Cartesian coordinate axes, θ is the effective porosity, t is time, and D_{xx}, D_{yy}, D_{xy}, and D_{yx} are the local hydrodynamic dispersion coefficients. These coefficients are defined as

$$\theta D_{xx}=\alpha_L\frac{V_x^2}{V}+\alpha_T\frac{V_y^2}{V}+\theta D_0 \quad (2a)$$

$$\theta D_{yy}=\alpha_T\frac{V_x^2}{V}+\alpha_L\frac{V_y^2}{V}+\theta D_0 \quad (2b)$$

$$\theta D_{xy}=\theta D_{yx}=\frac{(\alpha_L-\alpha_T)V_xV_y}{V} \quad (2c)$$

where α_L and α_T are the longitudinal and lateral dispersivity coefficients, V is the magnitude of the Darcy velocity, and D_0 is the coefficient of molecular diffusion. Note that we have neglected the source term in (1). This does not result in any loss of generality because the well boundary conditions can be treated separately in the finite element formulation.

For a homogeneous and isotropic aquifer with a fully-penetrating well doublet operating at constant flow rate, the Darcy velocity components may be determined from

$$V_x=-\frac{Q}{2\pi b}\left[\frac{x-x_0}{(x-x_0)^2+y^2}-\frac{x+x_0}{(x+x_0)^2+y^2}\right] \quad (3a)$$

$$V_y=-\frac{Qy}{2\pi b}\left[\frac{1}{(x-x_0)^2+y^2}-\frac{1}{(x+x_0)^2+y^2}\right] \quad (3b)$$

where Q is the flow rate of each well, b is the aquifer thickness, x_0 is half the well spacing, and it is assumed the origin of the coordinate axes (x, y) is at the center of the line joining the two wells and the x axis is oriented along this line.

We consider the situation corresponding to zero initial concentration in the aquifer and unit concentration boundary condition at the injection well. To investigate numerical difficulties associated with the standard Galerkin finite element solution in the two-dimensional Cartesian coordinate system, we simulated two cases of medium and small longitudinal dispersivity values. Physical data are given in Table 1 together with the grid and time step values. In each case, a zero value for the molecular diffusion coefficient was assumed. The values of flow parameters selected and the longitudinal dispersivity value of 0.294 cm correspond to a laboratory experimental condition described in *Hoopes and Harleman* [1967*a*]. The problem was solved using a rectangular grid consisting of 435 (29 × 15) nodes.

Numerical results obtained are compared in Figure 1 with the analytical solution of *Hoopes and Harleman* [1967*a*]. In Figure 1, c_p denotes the concentration at the discharging well, c_0 is the constant concentration at the recharging well, and t_D denotes the dimensionless time defined by $t_D = Qt/2\pi\theta bx_0^2$. As can be seen, the numerical solution exhibits mild oscillations in case 1, and unstable oscillations in case 2, where the small dispersivity value, $\alpha_L = 0.294$ cm, could not be accommodated by the chosen rectangular grid. We estimate that for case 2 one would need to use an extremely fine grid consisting of four to five thousand nodes to circumvent the numerical oscillations. An alternative way to reduce the oscillations is to apply an upstream weighting procedure [see *Huyakorn and Pinder*, 1983] in the x and y directions, but we found that this led to excessive numerical dispersion unless the grid selected was also refined. With the standard finite element formulation and direct matrix solution, the simulation cost becomes prohibitive for a such a refined grid having a large matrix bandwidth.

Although the example provided involves the simple situation of two-dimensional transport in a homogeneous and isotropic aquifer, it serves the purpose of indicating the need for a better numerical solution approach to handle cases where dispersivity values are small fractions of the well spacing. For this reason, we developed an improved finite element formulation performed in three-dimensional curvilinear coordinates. This formulation is amenable to highly efficient matrix solution algorithms, and is suitable for use in performing two-dimensional and three-dimensional analyses of

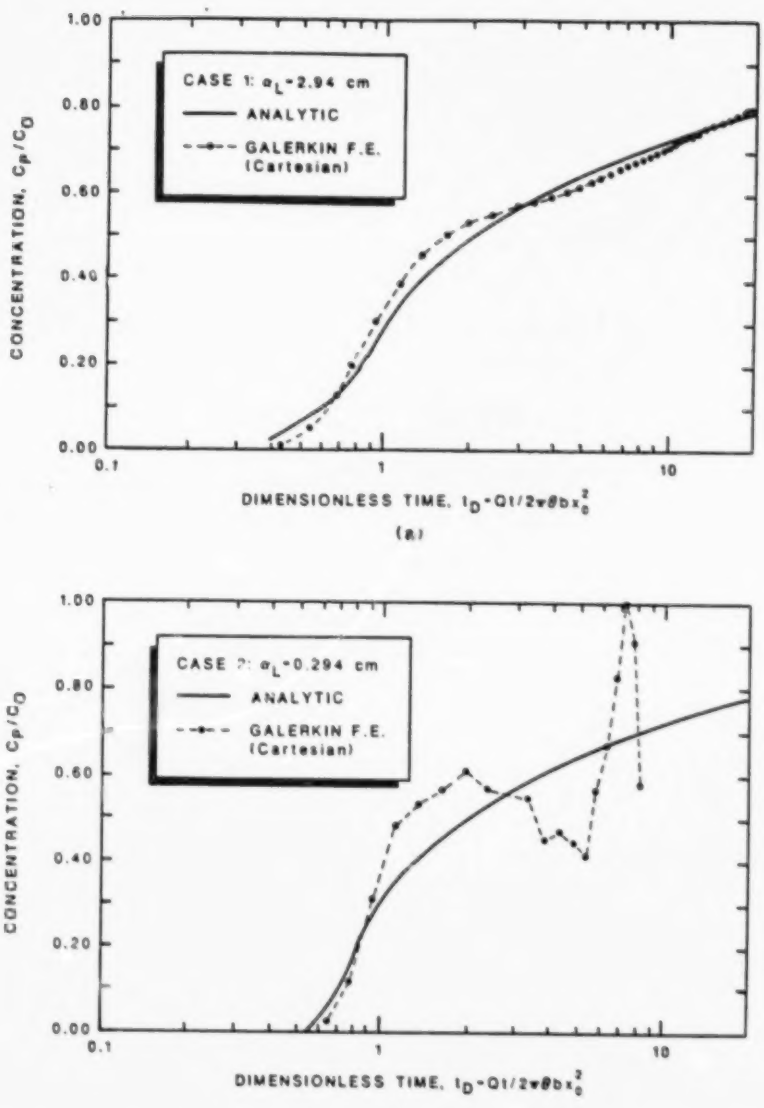

Fig. 1. Time versus concentration in the discharging well, showing comparison of analytical solution and finite element solution formulated in Cartesian coordinates.

two-well tracer tests in homogeneous and stratified (or layered) aquifers.

Equations in Curvilinear Coordinates

Consider a more general situation where the solute transport between the recharging and discharging well pair takes place in an isotropic stratified or layered aquifer. If the aquifer is perfectly stratified (areally homogeneous) and fully penetrated by both wells, the flow field may be considered planar. Consequently, the transport problem may be described using a converted form of the advective-dispersive equation written in three-dimensional curvilinear coordinates (s, n, z), where s and n are the coordinates along and normal to a local streamline, and z is the vertical coordinate. For an incremental flownet element, the required form of the transport equation is given by (for derivation, see Appendix A of this paper)

$$\frac{1}{h_2}\frac{\partial}{\partial s}\left(h_2 D_s \frac{\partial c}{\partial s}\right)+\frac{1}{h_1}\frac{\partial}{\partial n}\left(h_1 D_n \frac{\partial c}{\partial n}\right)+\frac{\partial}{\partial z}\left(D_z \frac{\partial c}{\partial z}\right) - \frac{V}{\theta}\frac{\partial c}{\partial s}-\frac{\partial c}{\partial t}=0 \qquad (4)$$

where D_s, D_n, and D_z are principal components of the hydrodynamic dispersion tensor in the longitudinal, transverse and vertical directions, respectively, and h_1 and h_2 are the scale factors of the curvilinear coordinate system. The dispersion coefficients are defined as

$$D_s = \alpha_L V/\theta + D_0 \qquad (5a)$$

$$D_n = \alpha_T V/\theta \qquad (5b)$$

$$D_z = \alpha_z V/\theta + D_0 \qquad (5c)$$

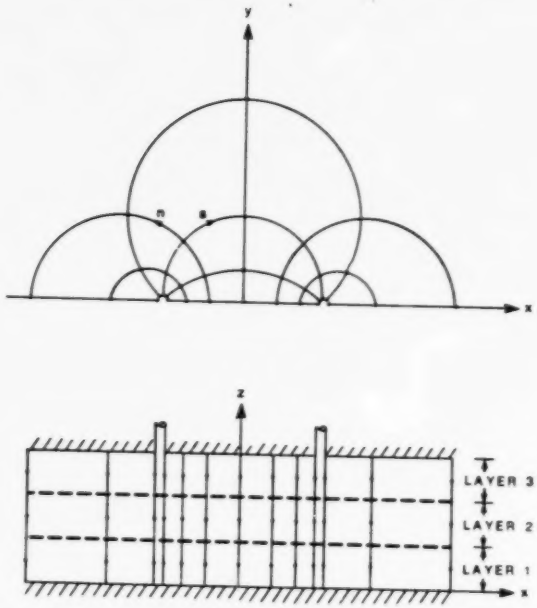

Fig. 2. Plan view and cross section of a typical three-dimensional curvilinear finite element grid.

where α_z is the vertical dispersivity, and V is a function of s, n, and z. The scale factors h_1 and h_2 are defined in Appendices A and B.

Note that in the simple case of two-dimensional transport in a homogeneous and isotropic aquifer, the z term in (4) vanishes and this equation then reduces to the converted form of (1). To convert the transport problem formulated in Cartesian coordinates to the corresponding one in the chosen curvilinear coordinates, we also need coordinate transformation relations. Because s and n are along and normal to streamlines, their relations with x and y can be determined using the equations for the stream function and the potential function, ψ and Φ. These equations are well established for the case of potential flow between a line source and a line sink [*Da Costa and Bennett*, 1960]. They can be written as [*Grove and Beetem*, 1971, *Hoopes and Harleman*, 1967*a*]

$$\frac{\psi}{A} = \tan^{-1}\left[\frac{2x_0 y}{x_0^2 - (x^2 + y^2)}\right] \tag{6}$$

and

$$\frac{\Phi}{A} = \frac{1}{2}\ln\left[\frac{(x + x_0)^2 + y^2}{(x - x_0)^2 + y^2}\right] \tag{7}$$

where A is a parameter that is layer-dependent. For a typical layer i of the stratified aquifer, A may be expressed as $A = Q_i/2\pi\theta b_i$, where Q_i is portion of the total flow rate, Q, that is transmitted through layer i, and b_i is the layer thickness; and the total flow rate Q is distributed to individual layers in proportion to their transmissivity values in accordance with the expression $Q_i = QK_ib_i/\sum_i K_ib_i$, hence A may be also expressed as $A = QK_i/2\pi\theta\sum_i K_ib_i$. Also note that for an isotropic aquifer, the potential function Φ is related to the hydraulic head, h, by $\Phi = -Kh/\theta$, where K is the hydraulic conductivity which, in the case of stratified (or layered) aquifer, is a function of z. From (6) and (7), the expressions for x and y may be obtained as

$$x = [x_0 \sinh(\Phi/A)]\beta \tag{8}$$

and

$$y = [x_0 \sin(\psi/A)]\beta \tag{9}$$

where

$$\beta = \cosh(\Phi/A) + \cos(\psi/A) \tag{10}$$

Note that β, Φ/A, and ψ/A are dimensionless and dependent only on x, y, and x_0. Knowing x and y from (8) and (9), we can determine s and n from the following equations:

$$ds = [(dx)^2 + (dy)^2]^{1/2}|_{\psi = \text{const}} \tag{11}$$

and

$$dn = [(dx)^2 + (dy)^2]^{1/2}|_{\Phi = \text{const}} \tag{12}$$

Finally, we need an expression for the magnitude of the Darcy velocity, V, which is also spatially dependent. This may be derived by using the definition $\Phi = -Kh/\theta$ together with (6) and Darcy's law. The required expression is given by [*Hoopes and Harleman*, 1967*a*]

$$V = \frac{\theta A}{x_0}[\cosh(\Phi/A) + \cos(\psi/A)] \tag{13a}$$

or

$$V = \theta A\beta/x_0 \tag{13b}$$

Finite Element Discretization

A three-dimensional finite element approximation of (4) is achieved in two steps by making a combined use of upstream weighted-residual and subdomain collocation procedures in the s-n space and in the z space, respectively. To construct the approximation, we first divide the three-dimensional aquifer region into layers and subdivide each layer into a number of orthogonal curvilinear elements as shown in Figure 2. Note that the same discretization pattern is used in the plan view for all layers, and the nodes are block-centered in the vertical z direction. Furthermore, it is assumed that within each layer the hydraulic conductivity is constant.

In the physical plane, the finite element network corresponds to the flow net depicted in Figure 3*a*. This flow net becomes a rectangular grid in the complex plane as illustrated in Figure 3*b*. (The complex plane will be used subsequently in the scheme for generating a curvilinear finite element network.) Note that there exist two singular points at $(\Phi/A, \psi/A) = (0, \pi)$ and $(\Phi/A, \psi/A) = (0, -\pi)$, which cannot be located in the physical plane. We now describe the two-step procedure of the proposed finite element formulation.

Step 1. Upstream Weighted-Residual Approximation in the s-n Space

The function $c(s, n, z, t)$ is represented by a trial function:

$$c \simeq \hat{c}(s, n, z, t) = N_j(s, n)c_j(z, t) \tag{14}$$

$$j = 1, 2, \cdots, n^*$$

where repeated indices indicate nodal summation, $N_j(s, n)$ are bilinear basis functions in the flow plane, $c_j(z, t)$ are nodal parameters that are functions of z and t, and n^* is the number of nodes in each layer. Next, we perform integration in the flow plane using the upstream-weighted residual procedure described in *Huyakorn and Nilkuha* [1979] and *Huyakorn and*

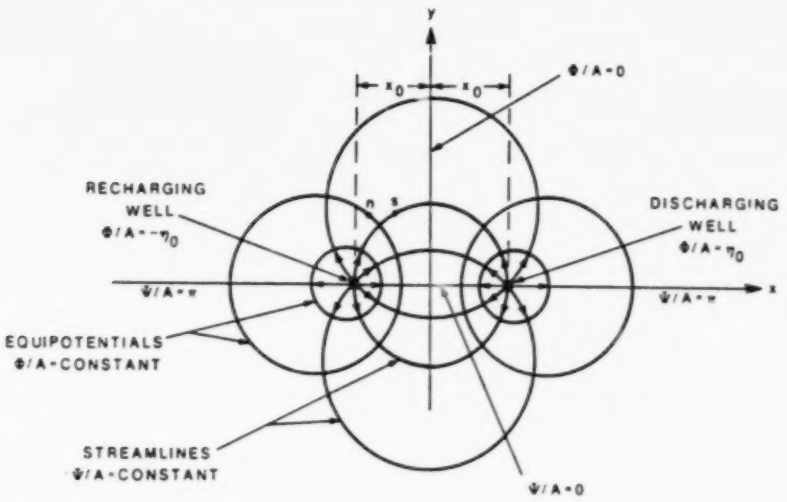

(a) PHYSICAL PLANE

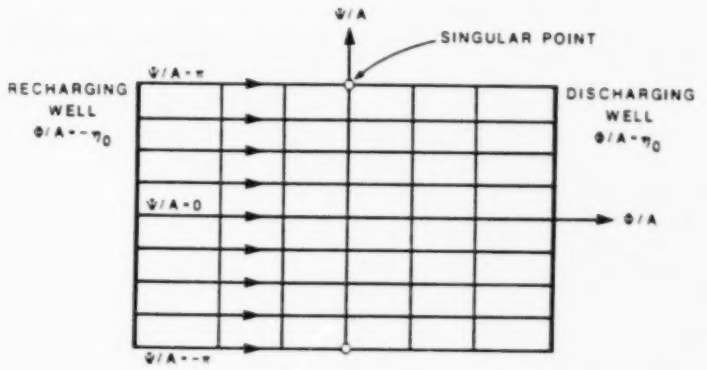

(b) COMPLEX PLANE

Fig. 3. Equipotential and streamline pattern for steady flow between recharging and discharging wells.

Pinder [1983]. This leads to the following set of integral equations (see Appendix B for details):

$$\int_R \left(D_s \frac{\partial W_I}{\partial s} \frac{\partial N_J}{\partial s} + D_n \frac{\partial W_I}{\partial n} \frac{\partial N_J}{\partial n} + \frac{V}{\theta} W_I \frac{\partial N_J}{\partial s} \right) dR\, c_J - \int_R (N_I N_J dR) \left[\frac{\partial}{\partial z} \left(D_z \frac{\partial c_J}{\partial z} \right) \right] + \int_R (N_I N_J dR) \frac{\partial c_J}{\partial t} - \int_B W_I \left(D_s \frac{\partial \hat{c}}{\partial s} v_s + D_n \frac{\partial \hat{c}}{\partial n} v_n \right) dB = 0 \qquad (15)$$

$$I = 1, 2, \cdots, n^*$$

where R is the region of integration in the flow plane, B is the boundary of R, W_I is used to denote asymmetric upstream weighting functions, and v_s and v_n are components of the outward unit vector normal to the boundary B.

Equation (15) can be written in the form

$$E_{IJ} c_J - B_{IJ} \frac{\partial}{\partial z} \left(D_z \frac{\partial c_J}{\partial z} \right) + B_{IJ} \frac{\partial c_J}{\partial t} - f_I = 0 \qquad (16)$$

$$I = 1, 2, \cdots, n$$

where

$$E_{IJ} = \sum_e E_{IJ}^e = \sum_e \int_{R^e} \left(D_s \frac{\partial W_I}{\partial s} \frac{\partial N_J}{\partial s} + D_n \frac{\partial W_I}{\partial n} \frac{\partial N_J}{\partial n} + \frac{V}{\theta} W_I \frac{\partial N_J}{\partial s} \right) dR \qquad (17a)$$

$$B_{IJ} = \sum_e B_{IJ}^e = \sum_e \int_{R^e} N_I N_J\, dR \qquad (17b)$$

$$f_I = \sum_e f_I^e = \sum_e \int_{B^e} W_I \left(D_s \frac{\partial \hat{c}}{\partial s} v_s + D_n \frac{\partial \hat{c}}{\partial n} v_n \right) dB \qquad (17c)$$

R^e is the element subregion enclosed by boundary B^e, and $\sum_e$

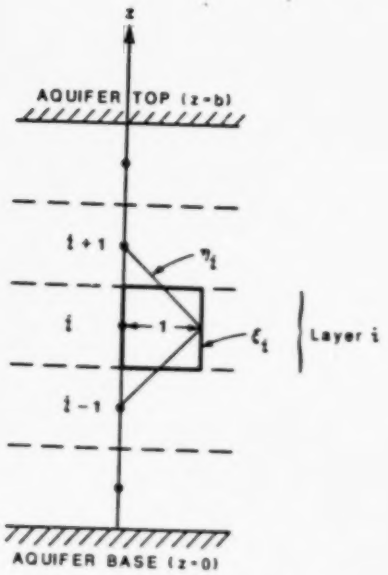

Fig. 4. Basis and weighting functions for typical node in layer i of the subdomain collocation in the z space.

is the summation over the number of curvilinear elements in each layer.

Step 2. Subdomain Collocation in the z Space

Equation (16) is a set of n^* partial differential equations having c_j as the dependent variables that are functions of z and t. The approximation of (16) in the z space is obtained using the subdomain collocation procedure [see *Lapidus and Pinder*, 1981]. Now we represent c_j by a trial function of the form

$$c_j(z, t) \simeq \hat{c}_j(z, t) = \eta_i(z)c_{ji}(t) \qquad j = 1, 2, \cdots, n' \qquad (18)$$

where $\eta_i(z)$ and $c_{ji}(t)$ are one-dimensional linear basis functions and nodal values of concentration at time t, respectively. The basis function for a typical node in layer i is depicted in Figure 4 together with the corresponding weighting function, ξ_i. Note that ξ_i is a unit function supporting $z_{i-1/2} \le z \le z_{i+1/2}$.

Applying the subdomain procedure with weighting function ξ_i to (16), one obtains the following set of weighted-residual equations:

$$\int_0^b \xi_i \left[E_{lj}\hat{c}_j - B_{lj}\frac{\partial}{\partial z}\left(D_{zz}\frac{\partial \hat{c}_j}{\partial z}\right) + B_{lj}\frac{\partial \hat{c}_j}{\partial t} - f_l \right] dz = 0 \qquad (19)$$

$$l = 1, 2, \cdots, n^* \qquad i = 1, 2, \cdots, n'$$

where b is the aquifer thickness.

Equation (19) can be further manipulated by performing ordinary integration and integration by parts to give

$$\int_{z_{i-1/2}}^{z_{i+1/2}} \left(E_{lj}c_j + B_{lj}\frac{\partial \hat{c}_j}{\partial t} - f_l \right) dz - \left[\left(B_{lj}D_{zz}\frac{\partial \hat{c}_j}{\partial z} \right)_{i+1/2} - \left(B_{lj}D_{zz}\frac{\partial \hat{c}_j}{\partial z} \right)_{i-1/2} \right] = 0 \qquad (20)$$

$$l = 1, 2, \cdots, n^* \qquad i = 1, 2, \cdots, n'$$

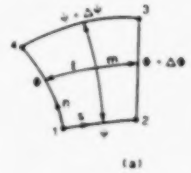

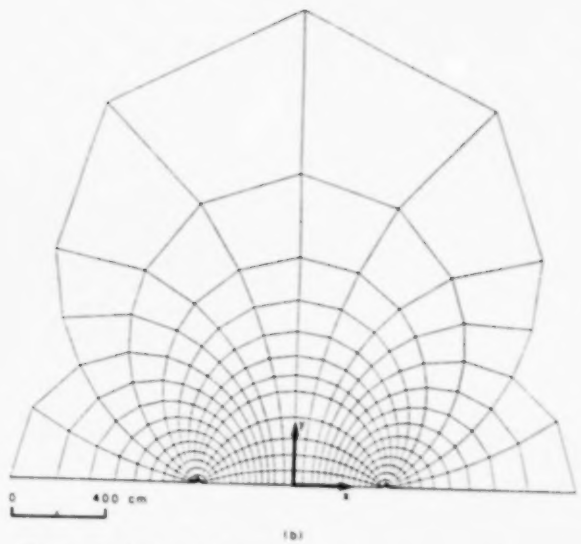

Fig. 5. Typical curvilinear finite element, and portion of the grid used in simulating laboratory experiment reported by *Hoopes and Harleman* [1967a].

For convenience in evaluating the integrals, we assume constant vertical nodal spacings of Δz. After combining (20) and (18) and integrating, the following equation is obtained for an internal nodal sublayer i:

$$\frac{\Delta z}{4}(E_{lj})(c_{j,i-1} + 2c_{ji} + c_{j,i+1}) + \left(\frac{\Delta z}{4}\right) B_{lj}\left(\frac{dc_{j,i-1}}{dt} + 2\frac{dc_{ji}}{dt} + \frac{dc_{j,i+1}}{dt}\right) - (\Delta z)(f_{li}) + \frac{B_{lj}}{\Delta z}\left[(D_{zz})_{i-1/2}(c_{ji} - c_{j,i-1}) - (D_{zz})_{i+1/2}(c_{j,i+1} - c_{ji})\right] = 0 \qquad (21)$$

The equations corresponding to the bottom and top boundary nodal layers can be derived in a similar manner. Equation (21) may be simplified by using the following matrix lumping approximation as follows:

$$\frac{\Delta z}{4}(c_{j,i-1} + 2c_{ji} + c_{j,i+1}) \simeq (\Delta z)c_{ji} \qquad (22)$$

$$\frac{\Delta z}{4}\left(\frac{dc_{j,i-1}}{dt} + 2\frac{dc_{ji}}{dt} + \frac{dc_{j,i+1}}{dt}\right) \simeq (\Delta z)\frac{dc_{ji}}{dt} \qquad (23)$$

Combining (21)–(23) gives

$$(\Delta z)\left[E_{lj}c_{ji} + B_{lj}\frac{dc_{ji}}{dt} - f_{li}\right]$$

$$+\frac{B_{IJ}}{\Delta z}\left[(D_{zz})_{i-1/2}(c_{JI}-c_{JI-1})-(D_{zz})_{i+1/2}(c_{JI+1}-c_{JI})\right]=0 \tag{24}$$

It is interesting to note that (24), which is a simplified form of the subdomain collocation approximation in the z space, is indeed a block-centered finite difference approximation of (16). This indicates a direct relationship between the subdomain finite element scheme and the conventional block-centered grid finite difference scheme in one-dimensional space.

Element Matrix Evaluation

For a typical orthogonal curvilinear element shown in Figure 5*a*, the element matrices can be evaluated by adapting the influence coefficient technique described in *Huyakorn et al.* [1985] for linear rectangular elements. First the element matrix $[E]^e$ is expressed as

$$[E]^e=[E_D]^e+[E_v{}^s]^e \tag{25}$$

where $[E_D]^e$ and $[E_v{}^s]^e$ are the contributions from the dispersive and the advective terms. The matrices $[E_D]^e$ and $[E_v{}^s]^e$ can be evaluated using the following influence coefficient formulas:

$$[E_D]^e=\langle D_L\rangle\frac{m}{l}[E_D{}^{ss}]^e+\langle D_T\rangle\frac{l}{m}[E_D{}^{nn}]^e \tag{26}$$

and

$$[E_v{}^s]^e=\langle V/\theta\rangle\frac{m}{2}([E_v{}^s]^e+[E_v{}^s]_u^e) \tag{27}$$

where $\langle D_L\rangle$, $\langle D_T\rangle$, and $\langle V/\theta\rangle$ are values of D_L, D_T, and V/θ evaluated at the element centroid, l and m are the average length and width of the curvilinear element, and $[E_D{}^{ss}]^e$, $[E_D{}^{nn}]^e$, and $[E_v{}^s]^e$ and $[E_v{}^s]_u^e$ are influence coefficient matrices corresponding to matrices $[E_D{}^{xx}]^e$, $[E_D{}^{yy}]^e$, $[E_v{}^x]^e$ and $[E_v{}^x]_u^e$ given in Appendices 1 and 2 of Huyakorn et al.

For the typical element in Figure 5*a*, the average length and width can be calculated from

$$l=\int_{\Phi}^{\Phi+\Delta\Phi}\left((\partial x/\partial\Phi)^2+(\partial y/\partial\Phi)^2\right)^{1/2}\Big|_{\Phi+\Delta\Phi/2}d\Phi \tag{28a}$$

$$m=\int_{\Psi}^{\Psi+\Delta\Psi}\left((\partial x/\partial\psi)^2+(\partial y/\partial\psi)^2\right)^{1/2}\Big|_{\Psi+\Delta\Psi/2}d\psi \tag{28b}$$

The remaining element matrix $[B]^e$ is a mass matrix given by

$$[B]^e=\frac{lm}{4}[M]^e \tag{29}$$

where $[M]^e$ is the influence coefficient matrix also given in Appendix 1 of *Huyakorn et al.* [1985].

Procedure for Upstream Weighting Along Streamlines

It should be noted that one advantage in using the orthogonal curvilinear finite element flow net is the perfect alignment of the direction of upstream weighting with the flow direction. This will lead to a significant reduction of numerical dispersion caused by application of upstream weighting. Recognizing the advantage of upstream weighting along the flow direction, several researchers have recently attempted to devise various procedures for achieving it. Typical examples include finite element and finite difference streamline upwinding methods presented by *Rosen* [1982], and *Hassan et al.* [1983], respectively.

In our computational scheme, the influence coefficient matrix $[E_v{}^s]^e$ is the one corresponding to the contribution of upstream weighting. It depends on a weighting factor known as upstream parameter, α. In the numerical simulation, the value of α is selected to be between 0 and 1. The zero value of α corresponds to no upstream weighting, and has the effect of reducing the upstream-weighted residual approximation to the Galerkin approximation in the s-n space. The unit value of α corresponds to full upstream weighting.

In using upstream weighting, our aim is to control oscillations without introducing excessive amounts of numerical dispersion. To achieve this, we designed a simple formula for automatic calculation of upstream parameter values to be applied to individual finite elements. This formula is given by

$$\begin{aligned}\alpha_e&=\alpha^*\left(1-\frac{2\alpha_L}{l}\right)\qquad l>2\alpha_L\\ \alpha_e&=0\qquad l\le 2\alpha_L\end{aligned} \tag{30}$$

where α^* is the assigned maximum allowable value of the upstream parameter, α_e is the value of α calculated for element e, α_L is the longitudinal dispersivity value, and l is the mean length of the element.

It is seen that according to (30), upstream weighting is applied only to those elements with local grid Peclet number (l/α_L) greater than 2. For such elements, the upstream parameter values are calculated such that when the element length becomes very large α_e approaches the assigned maximum allowable value, α^*. Our experience has shown that a value α^* between 0.1 and 0.2 is usually sufficient to control numerical oscillations, provided time step values are selected such that the Courant-Friedrichs criterion ($Vl/\Delta t\le 1$) is not grossly violated.

Time Stepping Schemes

Because the orthogonal curvilinear coordinate system selected results in an alignment of the finite element grid with the flow direction, time integration and solution of (24) can be performed conveniently using a noniterative alternating direction implicit (ADI) algorithm. For each time step, we perform three sweeps: (1) along the s direction (parallel to the flow), (2) along the n direction (transverse to the flow), and (3) along the z direction (normal to the flow plane). A general ADI scheme can be written by first expressing (24) in the form

$$(\Delta z)[E^s]+[E^n])\{c\}+(\Delta z)[B]\left\{\frac{dc}{dt}\right\}+[L]\{c\}=\{F\} \tag{31}$$

where $[E^s]$ and $[E^n]$ are portions of advective-dispersive matrix $[E]$ that contain derivatives with respect to the s and n coordinates, respectively, $[B]$ is the mass storage matrix, $[L]$ is a tridiagonal (vertical-dispersive) matrix derived from (24), and $\{F\}$ is a column vector containing $(\Delta z)f_{IJ}$.

The global matrices, $[E^s]$, $[E^n]$, $[B]$ and $\{F\}$, are evaluated by assembling element matrices of planar curvilinear elements. The ADI scheme is now performed in three stages as follows.

Stage 1. s sweep

$$\omega(\Delta z)[E^s]\{c\}^{k+1/3}+\frac{\Delta z[B]}{\Delta t}\{c\}^{k+1/3}=\frac{\Delta z[B]}{\Delta t}\{c\}^k$$
$$-(1-\omega)(\Delta z)[E^s]\{c^A\}-\Delta z[E^n]\{c\}^k-[L]\{c\}^k+\{F\}^{k+\omega} \tag{32}$$

Stage 2. n sweep

$$(\omega\Delta z)[E^n]\{c\}^{(k+1)**} + \frac{\Delta z[B]}{\Delta t}\{c\}^{(k+1)**}$$

$$= \frac{\Delta z[B]}{\Delta t}\{c\}^k - (1-\omega)\Delta z[E^n]\{c\}^k - \omega\Delta z[E^n]\{c\}^{(k+1)*}$$

$$- (1-\omega)\Delta z[E^s]\{c\}^k - [L]\{c\}^k + \{F\}^{k+\omega} \quad (33)$$

Stage 3. z sweep

$$\omega[L]\{c\}^{k+1} + \frac{\Delta z[B]}{\Delta t}\{c\}^{k+1}$$

$$= \frac{\Delta z[B]}{\Delta t}\{c\}^k - (1-\omega)[L]\{c\}^k$$

$$- \omega\Delta z[E^s]\{c\}^{(k+1)*} - (1-\omega)\Delta z[E^s]\{c\}^k$$

$$- \omega\Delta z[E^n]\{c\}^{(k+1)**} - (1-\omega)\Delta z[E^n]\{c\}^k + \{F\}^{k+\omega} \quad (34)$$

where $\{c\}^k$ contains concentration values at the old time level, $\{c\}^{(k+1)*}$ and $\{c\}^{(k+1)**}$ contain intermediate concentration values at the current time level, Δt is the time step value, ω is the time weighting factor, and $\{F\}^{k+\omega} = \omega\{F\}^k + (1-\omega)\{F\}^{k+1}$.

For stages 2 and 3, alternative equations can be obtained by subtracting (32) from (33) and (32) from (34), respectively. The resulting equations are given by

$$\Delta z\left(\omega[E^n] + \frac{[B]}{\Delta t}\right)\{c\}^{(k+1)**} = \Delta z\left(\omega[E^n]\{c\}^k + \frac{[B]}{\Delta t}\{c\}^{(k+1)*}\right) \quad (35)$$

and

$$\Delta z\left(\omega[L] + \frac{[B]}{\Delta t}\right)\{c\}^{k+1} = \Delta z\left(\omega[L]\{c\}^k + \frac{[B]}{\Delta t}\{c\}^{(k+1)**}\right) \quad (36)$$

The ADI algorithm presented above corresponds to the first-order temporal approximation scheme of *Douglas and Rachford* [1956] when ω is set to 1. It becomes the second-order temporal approximation scheme of *Douglas* [1962] when ω is set of $\frac{1}{2}$. Both schemes are highly stable. We prefer the Douglas Scheme because it provides a higher-order temporal approximation than the Douglas-Rachford Scheme. In each stage of the given ADI algorithm, tridiagonal subsets of algebraic equations are derived by evaluating global matrices $[E^s]$, $[E^n]$, and $[B]$ using the procedure described below for lumping element matrices.

$$[E^s]^e = \begin{bmatrix} e_{11}^s + e_{14}^s & e_{12}^s + e_{13}^s & 0 & 0 \\ e_{21}^s + e_{24}^s & e_{22}^s + e_{23}^s & 0 & 0 \\ 0 & 0 & e_{33}^s + e_{32}^s & e_{34}^s + e_{31}^s \\ 0 & 0 & e_{43}^s + e_{42}^s & e_{44}^s + e_{41}^s \end{bmatrix} \quad (37a)$$

and

$$[E^n]^e = \begin{bmatrix} e_{11}^n + e_{12}^n & 0 & 0 & e_{14}^n + e_{13}^n \\ 0 & e_{22}^n + e_{21}^n & e_{23}^n + e_{24}^n & 0 \\ 0 & e_{32}^n + e_{31}^n & e_{33}^n + e_{34}^n & 0 \\ e_{41}^n + e_{42}^n & 0 & 0 & e_{44}^n + e_{43}^n \end{bmatrix} \quad (37b)$$

where e_{ij}^s and e_{ij}^n are matrix elements of the original version of $[E^s]^e$ and $[E^n]^e$.

The element storage matrix $[B]^e$ can either be partially or fully lumped. For partial lumping, the structure of $[B]^e$ is made the same as that of $[E^s]^e$ in the s sweep, and it is made the same as that of $[E^n]^e$ in the n sweep. For full lumping, $[B]^e$ is diagonalized by summing across each row. Our experience indicates that full lumping of the element storage matrix leads to greater numerical stability than partial lumping. However, better accuracy is obtained with partial lumping, provided the numerical stability is maintained.

SOLUTION PROCEDURE

The overall strategy and solution procedure of the three-dimensional curvilinear finite element approach can be summarized as follows.

1. Divide the aquifer region into a number of layers and subdivide each layer into curvilinear flow-net finite elements. The finite element flow net can be constructed simply by performing conformal mapping from the complex plane to the physical plane (Figure 3). Briefly stated, the mapping procedure consists of two steps. First, the region in the complex plane is divided into rectangular elements with specified nodal values of Φ/A and ψ/A. Second, (8) and (9) are used to compute values of x and y for each pair of Φ/A and ψ/A values. In computing nodal coordinates and determining the element nodal connections in the physical plane, the two singular points and the elements connected to these points must be excluded. Because of symmetry, it is sufficient to deal with the upper half of the flow plane. Experience has shown that a finite element network yielding optimal accuracy is obtained by selecting values of Φ/A that lead to equal nodal spacings (in the physical plane) along the portion of x axis joining the two wells.

2. Evaluate element geometrical parameters and centroidal values of the seepage velocity. This is achieved by using (11), (12), (13*a*), (28*a*), and (28*b*).

3. For each time step, perform three successive ADI sweeps using (32), (35), and (36) with $\omega = \frac{1}{2}$. Each sweep requires the solution of tridiagonal subsets of algebraic equations by the Thomas algorithm. At the end of the third sweep, the corrected concentration values, $\{c\}^{k+1}$, are determined.

4. Compute the concentration in the discharging well, c_p^{k+1}, by first taking a weighted-average of contributions from the well boundary nodes in layer i and then taking the second weighted-average of contributions from individual layers. We use the following formulas:

$$c_{pi}^{k+1} = \sum_{s=1}^{n_\psi} \frac{1}{2\pi}(c_{pi,\psi_s}^{k+1} + c_{pi,\psi_{s+1}}^{k+1})\Delta\psi_s \quad (38)$$

$$c_p^{k+1} = \sum_{i=1}^{n'} d_{pi}^{k+1} Q_i/Q \quad (39)$$

where n_ψ is the number of streamlines in the upper-half flow plane, c_{pi,ψ_s} and $c_{pi,\psi_{s+1}}$ are c values at the well-boundary nodes in layer i and on streamlines ψ_s and ψ_{s+1}, respectively, $\Delta\psi_s = \psi_{s+1} - \psi_s$, c_{pi} is the weighted-averaged c value for layer i of the well boundary, b is the aquifer thickness, n' is the number of layers, and Q_i is the portion of the total flow rate Q that is distributed to layer i, given by $Q_i = Qb_iK_i/\sum_{i=1}^{n'} b_iK_i$.

5. To study the effect of stratification on concentration distribution, it is also desirable to compute vertically averaged concentration values at specified (x, y) locations. We use the

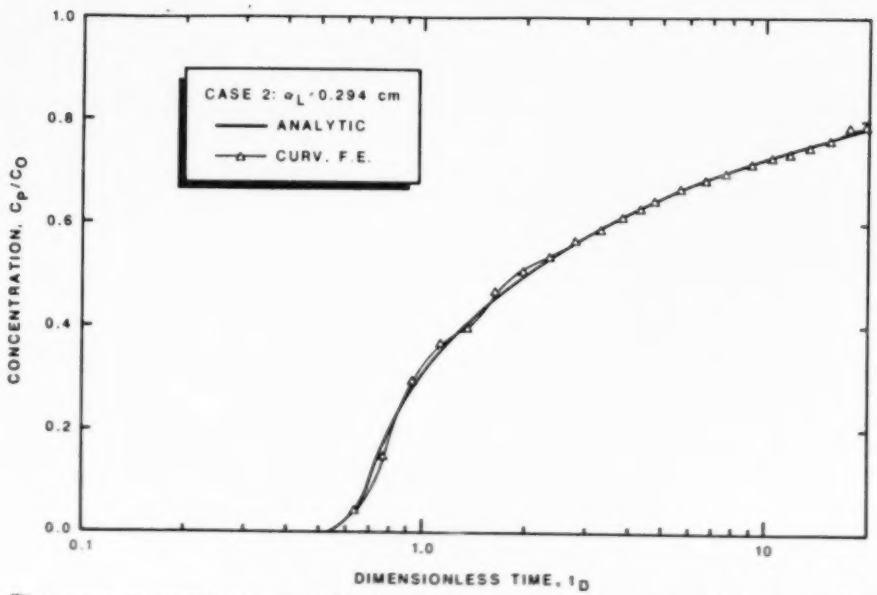

Fig. 6. Time versus concentration in the discharging well, showing comparison of analytical and curvilinear finite element solutions.

following flow-weighted averaging formula:

$$\bar{c}(x, y) = \frac{1}{Q} \sum_{i=1}^{m} c(x, y, z_i)Q_i \tag{40}$$

where $\bar{c}(x, y)$ is the flow-averaged concentration at (x, y) location.

GENERALIZATION

Although this paper focuses on the problem of solute transport in steady state two-dimensional flow created by a well doublet, the curvilinear finite element formulation presented can be generalized to handle other transport problems. We now provide a general discussion emphasizing two aspects. The first aspect concerns treatment of cases involving steady state potential flow fields that are too complicated to be determined analytically. The second aspect concerns extension of the numerical model to handle cases for which the key assumption of steady state two-dimensional flow is not justified.

Alternative Methods for Obtaining Curvilinear Flow Net

In a case where the potential flow field is too complicated to be determined analytically, the curvilinear finite element flow net can be constructed using one of the two following numerical approaches. The first approach involves the numerical solution of a pair of Laplace's equations describing the distributions ψ and Φ in the physical plane. The values of ψ and Φ so determined are then used to plot streamlines and equipotential lines.

The second approach is more elegant, involving conformal transformation and direct solution for nodal values of x and y, which are considered as the two dependent variables in the complex plane. The governing equations for x and y take the form

$$\frac{\partial^2 x}{\partial \Phi^2} + \frac{\partial^2 x}{\partial \psi^2} = 0 \tag{41}$$

$$\frac{\partial^2 y}{\partial \Phi^2} + \frac{\partial^2 y}{\partial \psi^2} = 0 \tag{42}$$

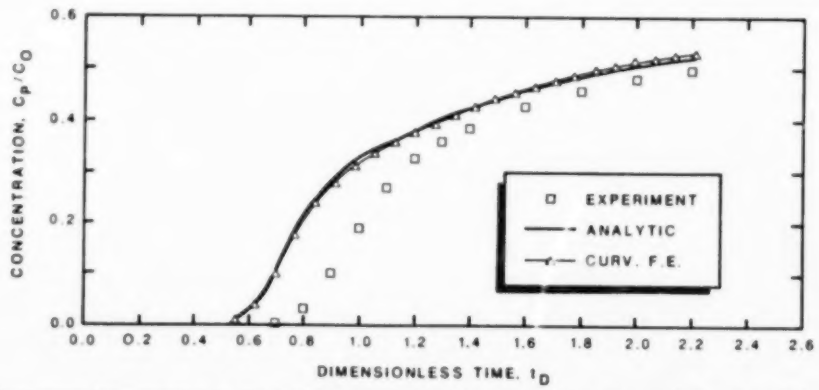

Fig. 7. Time versus concentration in the discharging well, showing comparison of numerical and analytical solutions versus experimental data.

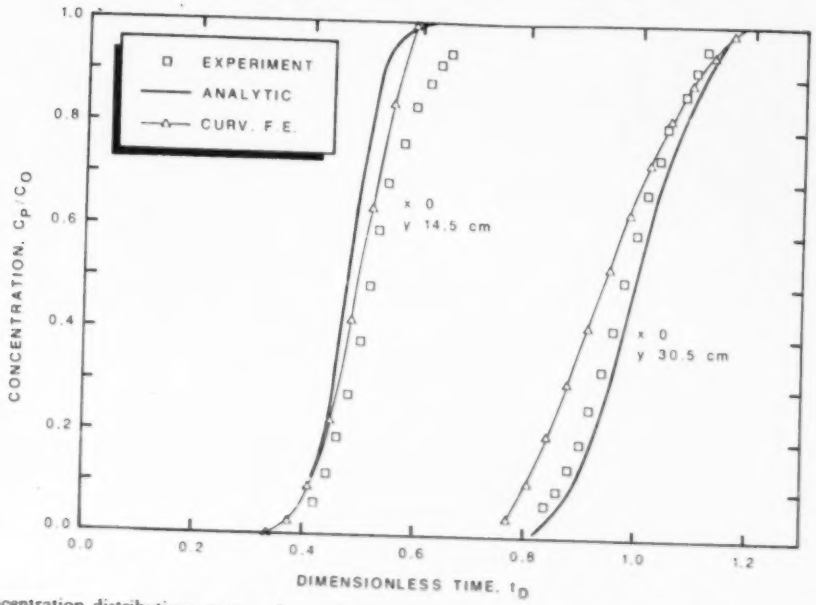

Fig. 8. Concentration distributions at two observation points on the y axis midway between the recharging and discharging wells.

Derivation and description of the numerical solution of (41) and (42) can be found in *Jeppson* [1968*a*].

We recommend the second numerical approach because it automatically provides a curvilinear finite element flow net that can be easily manipulated by adjusting values of $\Delta\Phi$ and $\Delta\psi$ in the complex plane. More difficult cases involving axisymmetric seepage in homogeneous and inhomogeneous media can also be treated via the technique described in *Jeppson* [1968*b*]. Once the desired curvilinear finite element network is obtained, the associated solute transport problem can then be solved in the same manner as described previously.

Extension of the Numerical Model

The curvilinear finite element model presented in the preceding sections may be viewed as a quasi-three-dimensional transport model because it requires the assumption of steady state planar flow of groundwater. There are many instances where this assumption may not be reasonable. Typical examples pertaining to a two-well tracer test are cases where (1) the test is performed using partially penetrating wells, (2) the flow rates of the recharging and the discharging well are unequal, and (3) the test is performed in an aquifer having large areal variations of hydraulic conductivity. To analyze such cases, it is necessary to extend the model. The extension is straightforward because of the manner in which spatial discretization is performed in our finite element formulation. There are three modifications to the model formulation that are needed. These are described briefly as follows.

1. In a general case where the chosen orthogonal curvilinear finite element grid is not in complete alignment with the flow direction, we need to replace (4) by a more general form of the transport equation. The latter can be found in *Bear* [1979, p. 244] and *Bachmat and Bear* [1964, p. 2564]. For completeness, we also present it in this paper as (B1) in Appendix B.

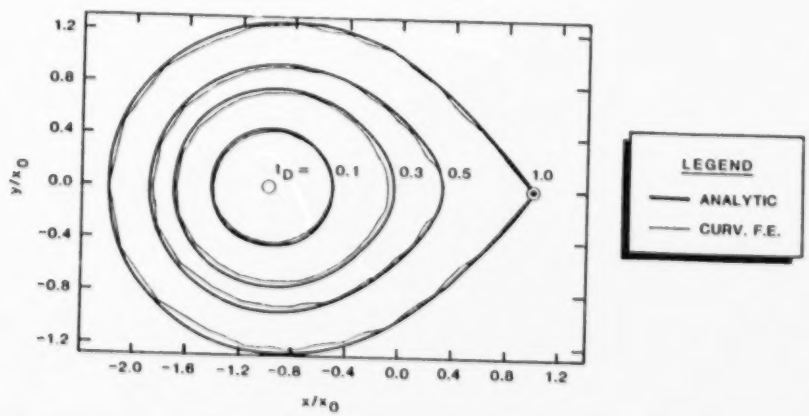

Fig. 9. Successive positions of solute front predicted by the present numerical model and the analytical model of *Muskat* [1937].

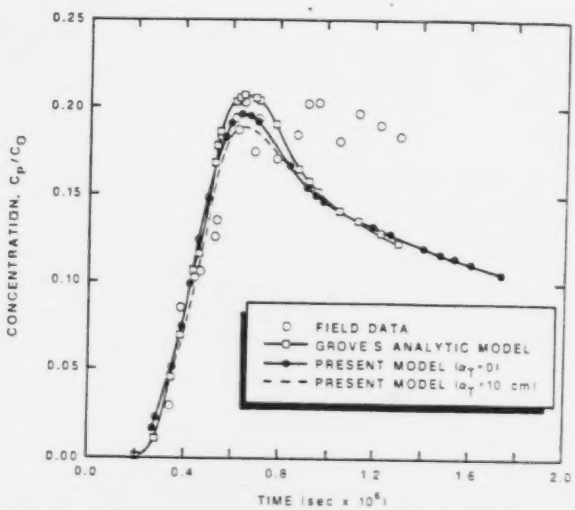

Fig. 10. Time versus concentration in the discharging well showing comparison field data from *Pickens and Grisak* [1981] and various simulation results.

2. As before, the three-dimensional finite element approximation is obtained by two successive applications of the upstream weighted residual procedure and the subdomain collocation procedure in the *s-n* space and the *z* space, respectively. The element matrix $[E]^e$ now contains additional terms associated with off-diagonal components of the hydrodynamic dispersion tensor as well as transverse and vertical velocity components. It can be evaluated in a simple manner using the influence coefficient technique with the incorporation of upstream weighting in the *s*, *n*, and *z* directions.

3. The global matrix equation resulting from the finite element approximation may still be represented by (24). Because of the extra terms in the global matrix $[E]$, we can no longer use the ADI algorithm to perform time stepping and matrix solution. To circumvent this problem, we now use the Alternate Layer and Line Sweep (ALALS) algorithm developed in *Huyakorn et al.* [1986*b*]. With the ALALS algorithm, the matrix solution for each time step is performed in two stages. The first stage involves a layer sweep or a layer-by-layer solution for the predicted values of concentration, and the second stage involves a vertical line sweep or a line-by-line solution for the corrected values of concentration. We wish to reiterate that the above modifications lead to the revised transport model that admits the use of an orthogonal curvilinear finite element grid that is not aligned with the flow direction. Despite this fact, it should be recognized that the orthogonal curvilinear finite element grid selected for the simulation should follow the pattern of groundwater in the modeled region as much as possible. This is because such a grid yields improved accuracy of the numerical solution by reducing numerical dispersion resulting from upstream weighting in the cross flow directions.

SIMULATION EXAMPLES

Two simulation examples are presented to show verification and validation of the curvilinear finite element model against the analytical solutions and laboratory and field experimental data for the well-doublet system. In the first example, the laboratory experiment reported by *Hoopes and Harleman* [1967*a*] was simulated. In the second example, the field experiment reported by *Pickens and Grisak* [1981] was simulated. Both examples concern two-dimensional simulations used to provide preliminary testing of our proposed numerical scheme, and demonstration of the computational advantages of the curvilinear finite element formulation. We deal with more elaborate three-dimensional field simulations and provide further demonstration of the utility of the model in the second paper of this series [*Huyakorn et al.*, 1986*a*].

Example 1. Laboratory Simulation

For this simulation, we used the physical parameter values in Table 1 (case 2). The case simulated corresponds to run 3 of the two-well nonrecirculating injection-withdrawal tracer test conducted in the laboratory at Massachusetts Institute of Technology. It should be recalled that for this case we obtained very poor numerical results using a 29 × 15 rectangular grid. To overcome the difficulty, a curvilinear grid was generated using the coordinate transformation relations given in (6)–(13) and the well radius of 0.5 cm. A major portion of the grid is illustrated in Figure 5*b*. This grid is a flow net consisting of 15 streamlines and 29 equipotential lines. It was generated using the following values of dimensionless stream function: ψ_j^* ($j = 1, 2, \cdots, 15$) = 0, 0.314, 0.628, 0.942, 1.26, 1.57, 1.78, 1.88, 2.04, 2.20, 2.36, 2.55, 2.75, 2.95, and 3.14 radians where $\psi_j^* = \psi_j / A$. The equipotential lines of the grid were placed such that they intersected the streamline joining the recharging and discharging wells at the following values of x coordinate: x_i ($i = 1, 2, \cdots, 29$) = −30, −28, −26, −24, −22, −20, −18, −16, −14, −12, −10, −8, −6, −3, 0, 3, 6, 8, 10, 12, 14, 16, 18, 20, 22, 24, 26, 28, and 30 cm.

The simulation was performed for 50 time steps using partial lumping of the element mass matrices. The time step values were calculated according to the algorithm given in Table 1. A small amount of upstream weighting (maximum upstream parameter, $\alpha^* = 0.1$) was needed to control minor numerical oscillations. Shown in Figure 6 is a plot of concentration versus time in the discharging well. It can be seen that there is good agreement between the analytical and numerical solutions. For completeness, the theoretical results are also compared in Figures 7 and 8 with experimental data. Note that the general shape of the experimental breakthrough curves is very similar to the theoretical curves at the same location. However, there is a time difference between the occurrence of the same value of the normalized concentration, c_p/c_0, as predicted theoretically and measured experimentally. It is pointed out in *Hoopes and Harleman* [1967*a*] that this difference was due to errors in the conductivity probe measurements. In Figure 8, concentration distributions at two observation points on the y axis midway between the recharging and discharging wells are plotted. The overall agreement between the theoretical and experimental results is also satisfactory. Note that at $y = 30.5$ cm, the numerical solution is slightly more dispersed than the analytical solution and the experimental data. This may be due to the effect of numerical dispersion. (The apparent numerical dispersion can be reduced by using smaller incremental values of stream function and potential functions in the vicinity of $y = 30.5$ cm.)

To provide further checking of the numerical solution, successive positions of the solute front corresponding to 0.5 isochlor are plotted in Figure 9. The selected dimensionless time values of 0.1, 0.3, 0.5 and 1 correspond to the real time values of 832, 2496, 4159 and 8318 s, respectively. The numerical solution is compared with the sharp-front (or pure advection)

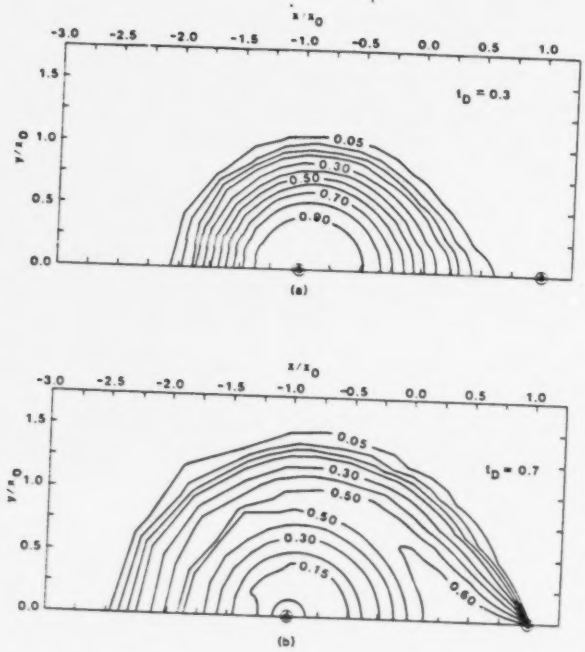

Fig. 11. Sequence of concentration contours obtained from the curvilinear finite element simulation of the field experiment, case 1, zero lateral dispersivity.

analytical solution of *Muskat* [1937]. As depicted in Figure 9, there is fairly good agreement between the numerical and analytical model results.

Example 2. Field Simulation

In this example, we performed the simulation of a two-well recirculating field tracer test. The field data were obtained from the test conducted at a site located near the Chalk River Nuclear Laboratories, Canada. A detailed description of this test and the instrumentation can be found in *Pickens and Grisak* [1981].

In brief, the test was conducted in a sand aquifer that exhibits significant vertical variation and some areal variation in hydraulic conductivity [see Figure 10 of *Pickens and Grisak*, 1981]. The average thickness of the aquifer is approximately 8.2 m for the monitored cross section. The recharging and discharging wells were spaced at a distance of 8 m. The fluid flow rate of each well was maintained constant at 4.49×10^{-4} m^3/s (0.499 L/s) through the entire test duration of 15 days. Tracer injection occurred over the initial period of 3.22 days.

For comparative purposes, we used a longitudinal dispersivity value of 50 cm and effective porosity of 0.38. The dispersivity value was determined by Pickens and Grisak from calibration of the stream tube analytical model presented by *Grove* (1971) and *Grove and Beetem* [1971]. Note that this analytical model is based upon the one-dimensional analytical solution given by *Brenner* [1962]. Furthermore, it cannot take into account lateral dispersion effects. In addition, we found that Grove's analytical computer code did not perform well for cases of small longitudinal dispersivity values such as those in example 1.

In view of the fact that the present numerical model can account for lateral dispersion, we simulated two cases: one for zero lateral dispersivity and the other for a lateral dispersivity value of 10 cm. The intention was to examine the effect of lateral dispersivity on concentration distributions.

A curvilinear grid comprised of 16 streamlines and 31 equipotential lines was set up. For this grid, the radius of each well was assumed as 4 cm. The following values of dimensionless stream function were selected: ψ_j^* ($j = 1, 2, \cdots, 16$) = 0, 0.131, 0.262, 0.393, 0.524, 0.785, 1.05, 1.31, 1.57, 1.77, 1.96, 2.16, 2.36, 2.62, 2.88, and 3.14 radians. The values of dimensionless equipotential function were selected such that the spacing between

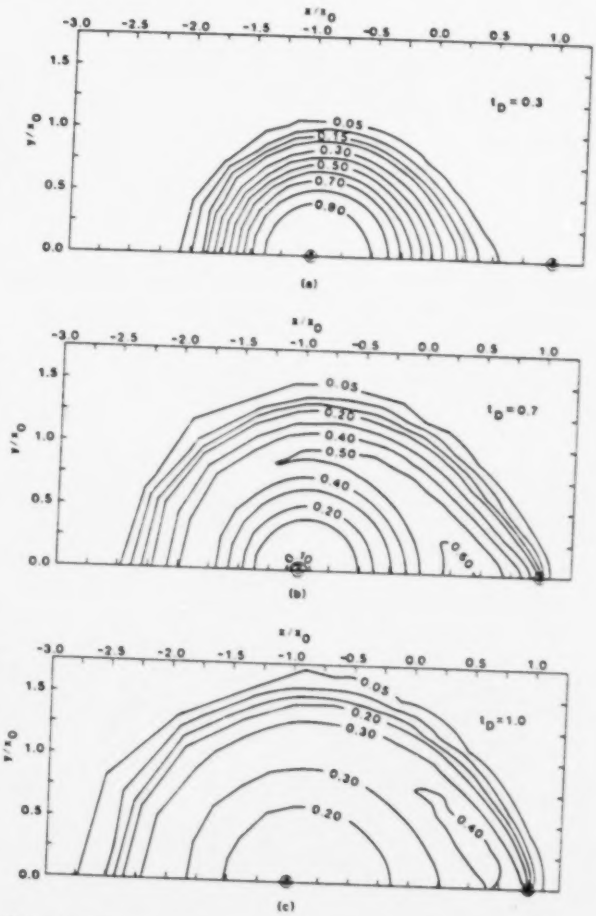

Fig. 12. Sequence of concentration contours obtained from the curvilinear finite element simulation of the field experiment, case 2, lateral dispersivity, $a_T = 10$ cm.

both wells was divided into 30 equal increments. The simulation was performed for 60 time steps. Once again, we used partial mass lumping and set the upstream parameter value to 0.1. The time stepping was started with an initial step of 70 s, the time step size was then gradually increased to a maximum value of 7×10^4 s to reach the final simulation time of 1.73×10^6 s (20 days).

Shown in Figure 10 is a plot of time versus normalized concentration in the pumping well. Included in this plot are the field experimental data and theoretical predictions from Grove's analytical model and the present model with transverse dispersivity values of 0 and 10 cm. All of the predicted (or theoretical) breakthrough curves were obtained taking recirculation into account. As can be seen from Figure 10, the model predictions agree satisfactorily with the field data up to $t = 0.8 \times 10^6$ s (9.26 days). At later time values, the field data points lie well above the predicted breakthrough curves. The reasons for this behavior are not entirely clear. The deviation of the model predictions from the field data may be in part due to the existence of stratification and some areal variation in the hydraulic conductivity of the aquifer at the site, which was ignored by both the analytical and the numerical models. It may also be noted from Figure 10 that using the lateral dispersivity of 10 cm resulted in a slight lowering of the average concentration in the pumping well up to $t = 0.9 \times 10^6$ seconds. At later time values, the effect of lateral dispersivity becomes negligible. For completeness, we also show the influence of lateral dispersivity on spatial distributions of concentration. Shown in Figures 11 and 12 are plots of concentration contours obtained from case 1 and 2. The time values selected for these plots correspond to $t_D = 0.3$, 0.7, and 1 or $t = 2.423$, 5.653, and 8.075 days, respectively. It is interesting to note that at early time, $t = 2.423$ days, during the tracer injection period, lateral dispersion has little effect on the spatial distribution of concentration. However, at later time values of 5.653 and 8.075 days, after the tracer injection has ceased, there are some differences in the predicted concentration distributions obtained with $\alpha_T = 0$ and $\alpha_T = 10$ cm. Evidently, lateral dispersion leads to slight reduction of concentration peaks, particularly at $t = 8.075$ days.

In comparing the simulation results with the field data, there is another important point that should be emphasized. This concerns the 50 cm value of longitudinal dispersivity obtained from model calibrations. This value represents a full-aquifer dispersivity value rather than a local dispersivity value. The latter varies over the aquifer thickness and, according to *Pickens and Grisak* [1981], ranges from 0.4 to 1.5 cm. Such a big difference (two orders of magnitude) between the full-aquifer and the local dispersivity values may be largely attributed to stratification of hydraulic conductivity, which is neglected by the one- and two-dimensional models considered so far. Hydraulic conductivity stratification causes lateral spreading of the plume and large apparent dispersion when the effects are averaged over the aquifer thickness. Further discussion of the physical implications of hydraulic conductivity stratification as related to the Pickens and Grisak data can be found in *Güven et al.* [1985, 1986]. For our purpose, it is sufficient to make the following statements pertaining to the case simulated. When the vertical variation in hydraulic conductivity is neglected in the simulation, it is necessary to rely on the full-aquifer longitudinal dispersivity to reproduce the hydrodynamic dispersion effects observed in the field. The main disadvantage in doing so is the fact that the full-aquifer dispersivity value determined from model calibration is scale-dependent. As pointed out by *Pickens and Grisak* [1981, p. 1209], the given dispersivity value (50 cm) is representative for describing transport in the aquifer only for situations with full-aquifer groundwater sampling instrumentation (fully penetrating wells) and with the same distance between input and sampling locations (8 m).

Discussion and Conclusions

The examples presented provide preliminary verification and validation of the finite element model developed to simulate two-well tracer tests. Of particular interest here is the fact that the proposed upstream weighted residual formulation in curvilinear coordinates is superior in terms of accuracy and computational efficiency to the standard Galerkin formulation in Cartesian coordinates. The latter cannot handle cases of small longitudinal dispersivity to well spacing ratios without requiring excessive computational cost. For comparative purposes, we provide the following information pertaining to the CPU time. To complete the field simulation reported, the present formulation with the ADI (Alternating Direction Implicit) algorithm took only 125 CPU s on the PRIME 550-II minicomputer using a coarse grid containing 496 (31×16) nodes and 60 time steps. The Galerkin formulation with a direct banded matrix solver took 1500 CPU s to perform the same simulation. This is already a difference of an order of magnitude in CPU time requirement even in the two-dimensional situation where the grid is coarse and the matrix bandwidth for the direct solver is rather small. In cases involving the use of very refined grids, the difference in CPU performance between the two algorithms can be expected to be more drastic because of large increases in matrix bandwidth for the direct matrix solution. (Note that the CPU time required by the ADI algorithm is proportional to the number of nodes, whereas the CPU time required by the direct matrix solver is proportional to the number of nodes times the square of the matrix bandwidth.)

The two simulation examples given in this paper have also served the purpose of providing a basis for testing the curvilinear finite element model in two dimensions. In particular, the second example indicates the need to investigate the impact of hydraulic conductivity stratification on results of two-well tracer tests in layered or stratified aquifer systems. Recognizing this need, we have conducted more elaborate three-dimensional simulations allowing for vertical variation in hydraulic conductivity. These simulations, which require the use of small local dispersivity values, have been made for two-well tracer tests conducted at two separate sites. These include the Chalk River site and one other site located in Mobile, Alabama. Results of our three-dimensional simulation study are presented in the second paper of this series.

Finally, we wish to emphasize that the curvilinear finite element formulation developed in this paper has general applicability, and should not be viewed as limited to the situation concerning two-well tracer tests. Indeed, the model formulation and solution strategy can be directly applied or readily adapted to a variety of groundwater contamination and solute transport scenarios. In particular, the formulation is well suited for those cases requiring the use of elaborate grids or dispersivity values that are very small compared to the physical scales of the transport problems.

APPENDIX A

In this appendix, we provide a simple derivation of the transport equation in curvilinear coordinates (s, n, z). Consider an incremental volume of the flow field shown in Figure 13. The mass conservation requirement for transport through this elementary volume may be expressed as (see also *Hoopes and Harleman*, 1967*b*]:

$$\frac{\partial}{\partial s}\left(\theta D_s \frac{\partial c}{\partial s}\Delta n\Delta z\right)\Delta s + \frac{\partial}{\partial n}\left(\theta D_n \frac{\partial c}{\partial n}\Delta s\Delta z\right)\Delta n + \frac{\partial}{\partial z}\left(\theta D_z \frac{\partial c}{\partial z}\Delta s\Delta n\right)\Delta z - \frac{\partial}{\partial s}(Vc\Delta n\Delta z)\Delta s = \frac{\partial}{\partial t}\theta c\Delta s\Delta n\Delta z \quad \text{(A1)}$$

where D_s, D_n, and D_z are dispersion coefficients defined in (5*a*)-(5*c*), V is the magnitude of Darcy velocity, and θ is the effective porosity. Since Δs, Δn, and Δz are independent of t, and $\partial(V\Delta n)/\partial s = 0$ for steady incompressible flow, (A1) reduces to

$$\frac{\partial}{\partial s}\left(\theta D_s \frac{\partial c}{\partial s}\Delta n\right)\Delta z\Delta s + \frac{\partial}{\partial n}\left(\theta D_n \frac{\partial c}{\partial n}\Delta s\right)\Delta z\Delta n + \frac{\partial}{\partial z}\left(\theta D_z \frac{\partial c}{\partial z}\Delta s\Delta n\right)\Delta z - V\frac{\partial c}{\partial s}\Delta n\Delta z\Delta s = \theta\frac{\partial c}{\partial t}\Delta s\Delta n\Delta z \quad \text{(A2)}$$

where we make use of the fact that Δz is independent of s and n.

Equation (A2) may be rearranged to give

$$\frac{1}{\Delta n}\frac{\partial}{\partial s}\left(D_s\frac{\partial c}{\partial s}\Delta n\right) + \frac{1}{\Delta s}\frac{\partial}{\partial n}\left(D_n\frac{\partial c}{\partial n}\Delta s\right) + \frac{1}{\Delta s\Delta n}\frac{\partial}{\partial z}\left(D_z\frac{\partial c}{\partial z}\Delta s\Delta n\right) - \frac{V}{\theta}\frac{\partial c}{\partial s} = \frac{\partial c}{\partial t} \quad \text{(A3)}$$

The arc lengths, Δs and Δn, of the elementary volume may be expressed in terms of the increments of potential and stream functions, $\Delta\Phi$ and $\Delta\psi$, as follows:

$$\Delta s = h_1\Delta\Phi \quad \text{(A4)}$$

$$\Delta n = h_2\Delta\psi \quad \text{(A5)}$$

where h_1 and h_2 are scale factors defined as

$$h_1 = \left[\left(\frac{\partial x}{\partial\Phi}\right)^2 + \left(\frac{\partial y}{\partial\Phi}\right)^2\right]^{1/2} \quad \text{(A5)}$$

$$h_2 = \left[\left(\frac{\partial x}{\partial\psi}\right)^2 + \left(\frac{\partial y}{\partial\psi}\right)^2\right]^{1/2} \quad \text{(A6)}$$

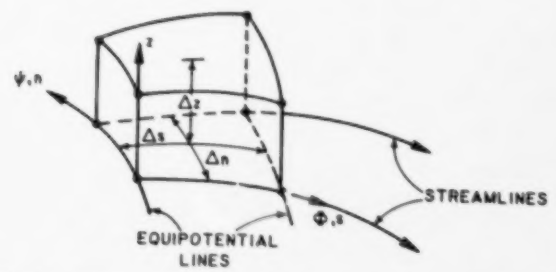

Fig. 13. Incremental volume of the flow field in curvilinear coordinate system.

Inserting (A4) and (A5) in (A3) and making use of the fact that $\Delta\Phi$ and $\Delta\psi$ are independent of s, n, and z, we obtain

$$\frac{1}{h_2}\frac{\partial}{\partial s}\left(h_2D_s\frac{\partial c}{\partial s}\right) + \frac{1}{h_1}\frac{\partial}{\partial n}\left(h_1D_n\frac{\partial c}{\partial n}\right) + \frac{1}{h_1h_2}\frac{\partial}{\partial z}\left(h_1h_2D_z\frac{\partial c}{\partial z}\right) - \frac{V}{\theta}\frac{\partial c}{\partial s} = \frac{\partial c}{\partial t} \quad \text{(A7)}$$

For perfectly stratified flow, we note that h_1 and h_2 are independent of z and hence (A7) reduces to

$$\frac{1}{h_2}\frac{\partial c}{\partial s}\left(h_2D_s\frac{\partial c}{\partial s}\right) + \frac{1}{h_1}\frac{\partial c}{\partial n}\left(h_1D_n\frac{\partial c}{\partial n}\right) + \frac{\partial}{\partial z}\left(D_z\frac{\partial c}{\partial z}\right) - \frac{V}{\theta}\frac{\partial c}{\partial s} - \frac{\partial c}{\partial t} = 0 \quad \text{(A8)}$$

APPENDIX B

In this appendix, we show that (A8) can also be obtained using the general form of the fully three-dimensional transport equation written in an arbitrary orthogonal curvilinear coordinate system (ξ^1, ξ^2, ξ^3). We also provide details on the manipulation of the integrals resulting from the weighted residual approximation of (A4) in the s-n space.

The general form of the transport equation in orthogonal curvilinear coordinates can be found in *Bachmat and Bear* [1964, p. 2564] and *Bear* [1979, p. 245]. In our notation, it can be written as

$$\frac{1}{h_1h_2h_3}\frac{\partial}{\partial\xi^i}\left\{\frac{h_1h_2h_3}{(h_i)^2}\left[(\alpha_L-\alpha_T)\frac{V_iV_k}{V}\frac{1}{(h_k)^2}\frac{\partial c}{\partial\xi^k} + \alpha_T V\frac{\partial c}{\partial\xi^i} + D_0\frac{\partial c}{\partial\xi^i}\right]\right\} - \frac{V_i}{(h_i)^2}\frac{\partial c}{\partial\xi^i} = \theta\frac{\partial c}{\partial t} \quad \text{(B1)}$$

where the tensorial summation convention is applied to terms other than h_i^2 and h_k^2, and h_1, h_2, and h_3 are the scale factors of the curvilinear system and are defined as

$$h_i^2 = \left(\frac{\partial x^1}{\partial\xi^i}\right)^2 + \left(\frac{\partial x^2}{\partial\xi^i}\right)^2 + \left(\frac{\partial x^3}{\partial\xi^i}\right)^2 \quad \text{(B2)}$$

with x^1, x^2, and x^3 being the Cartesian coordinates.

In our situation of transport in perfectly stratified flow, the coordinates ξ^1, ξ^2, and ξ^3 correspond to Φ, ψ, and z, respectively. Thus, $V_1 = h_1V \neq 0$, and $V_2 = V_3 = 0$, and (B2) reduces to

$$\frac{1}{h_1h_2h_3}\left\{\frac{\partial}{\partial\Phi}\left[\frac{h_1h_2h_3}{(h_1)^2}\left((\alpha_L-\alpha_T)\frac{V_1^2}{Vh_1^2}\frac{\partial c}{\partial\Phi} + (\alpha_TV+D_0)\frac{\partial c}{\partial\Phi}\right)\right] + \frac{\partial}{\partial\psi}\left[\frac{h_1h_2h_3}{(h_2)^2}(\alpha_TV+D_0)\frac{\partial c}{\partial\psi}\right] + \frac{\partial}{\partial z}\left[\frac{h_1h_2h_3}{(h_3)^2}(\alpha_TV+D_0)\frac{\partial c}{\partial z}\right]\right\} - \frac{V_1}{(h_1)^2}\frac{\partial c}{\partial\Phi} = \theta\frac{\partial c}{\partial t} \quad \text{(B3)}$$

where h_1 and h_2 are defined by (A5) and (A6) and $h_3 = 1$. Equation (B3) may be simplified to give

$$\frac{1}{h_1h_2}\left\{\frac{\partial}{\partial\Phi}\left[\frac{h_2}{h_1}(\alpha_LV+D_0)\frac{\partial c}{\partial\Phi}\right] + \frac{\partial}{\partial\psi}\left[\frac{h_1}{h_2}(\alpha_TV+D_0)\frac{\partial c}{\partial\psi}\right] + \frac{\partial c}{\partial z}\left[h_1h_2(\alpha_TV+D_0)\frac{\partial c}{\partial z}\right]\right\} - \frac{V}{h_1}\frac{\partial c}{\partial\Phi} = \theta\frac{\partial c}{\partial t} \quad \text{(B4)}$$

Equation (B4) may be written in terms of the arc-length coordinate system (s, n, z) using the relations $ds = h_1d\Phi$ and $dn =$

$h_2 d\psi$. Thus, we obtain

$$\frac{1}{h_2}\frac{\partial}{\partial s}\left[h_2\left(\alpha_L\frac{V}{\theta}+D_0\right)\frac{\partial c}{\partial s}\right]+\frac{1}{h_1}\frac{\partial}{\partial n}\left[h_1\left(\alpha_T\frac{V}{\theta}+D_0\right)\frac{\partial c}{\partial n}\right]+\frac{1}{h_1h_2}\frac{\partial}{\partial z}\left[h_1h_2\left(\alpha_T\frac{V}{\theta}+D_0\right)\frac{\partial c}{\partial z}\right]-\frac{V}{\theta}\frac{\partial c}{\partial s}=\frac{\partial c}{\partial t} \quad \text{(B5)}$$

which, if we adopt the definitions $D=\alpha_L V/\theta+D_0$, $D_n=\alpha_T V/\theta+D_0$, and $D_z=\alpha_T V/\theta+D_0$, becomes identical to equation (A7). Since h_1 and h_2 are independent of z, (B5) also reduces to (A8).

In our finite element formulation, (A8) is discretized in the (s-n) space using the upstream weighted residual procedure presented by *Huyakorn and Nilkuha* [1979]. With this procedure, the s and n terms of (A8) are weighted by asymmetric weighting functions W_I and the remaining terms are weighted using the basis functions N_I. Thus, we obtain

$$\int_R W_I\left[\frac{1}{h_2}\frac{\partial\hat{c}}{\partial s}\left(h_2 D_s\frac{\partial\hat{c}}{\partial s}\right)+\frac{1}{h_1}\frac{\partial\hat{c}}{\partial n}\left(h_1 D_n\frac{\partial\hat{c}}{\partial n}\right)-\frac{V}{\theta}\frac{\partial\hat{c}}{\partial n}\right]ds\,dn+\int_R N_I\left[\left(D_z\frac{\partial\hat{c}}{\partial z}\right)-\frac{\partial\hat{c}}{\partial t}\right]ds\,dn=0 \qquad I=1,2,\cdots,n^* \quad \text{(B6)}$$

where $\hat{c}$ is the trial function defined by (14). Noting that $dn=h_2\,d\psi$ and taking advantage of Green's theorem, we can write

$$\int_R W_I\left[\frac{1}{h_2}\frac{\partial\hat{c}}{\partial s}\left(h_2 D_s\frac{\partial\hat{c}}{\partial s}\right)\right]ds\,dn=\int_R W_I\frac{\partial\hat{c}}{\partial s}\left(h_2 D_s\frac{\partial\hat{c}}{\partial s}\right)ds\,d\psi=-\int_R D_s\frac{\partial W_I}{\partial s}\frac{\partial\hat{c}}{\partial s}\,ds\,(h_2\,d\psi)+\int_B W_I\left(D_s\frac{\partial\hat{c}}{\partial s}v_s\right)dB \quad \text{(B7)}$$

Equation (B7) can be written in the form

$$\int_R W_I\left[\frac{1}{h_2}\frac{\partial\hat{c}}{\partial s}\left(h_2 D_s\frac{\partial\hat{c}}{\partial s}\right)\right]ds\,dn=-\int_R D_s\frac{\partial W_I}{\partial s}\frac{\partial\hat{c}}{\partial s}\,dR+\int_B W_I\left(D_s\frac{\partial\hat{c}}{\partial s}v_s\right)dB \quad \text{(B8)}$$

where $dR=ds\,dn$.

Similarly, we can also write

$$\int_R W_I\left[\frac{1}{h_1}\frac{\partial\hat{c}}{\partial n}\left(h_1 D_n\frac{\partial\hat{c}}{\partial n}\right)\right]ds\,dn=-\int_R D_n\frac{\partial W_I}{\partial n}\frac{\partial\hat{c}}{\partial n}\,dR+\int_B W_I\left(D_n\frac{\partial\hat{c}}{\partial n}v_n\right)dB \quad \text{(B9)}$$

Inserting (B8) and (B9) in (B6), replacing $\hat{c}$ by $N_J c_J$, and rearranging the terms, we obtain

$$\int_R\left(D_s\frac{\partial W_I}{\partial s}\frac{\partial N_J}{\partial s}+D_n\frac{\partial W_I}{\partial n}\frac{\partial N_J}{\partial n}+\frac{V}{\theta}W_I\frac{\partial N_J}{\partial s}\right)dR\,c_J-\int_R(N_I N_J\,dR)\left[\frac{\partial}{\partial z}\left(D_z\frac{\partial c_J}{\partial z}\right)\right]+\int_R(N_I N_J\,dR)\frac{\partial c_J}{\partial t}-\int_B W_I\left(D_s\frac{\partial\hat{c}}{\partial s}v_s+D_n\frac{\partial\hat{c}}{\partial n}v_n\right)dB=0 \quad I=1,2,\cdots,n^* \quad \text{(B10)}$$

which is identical to (15) in the main text.

NOTATION

A	flow parameter defined as $A=Q_i/2\pi\theta b_i$, L^2T^{-1}.
b	aquifer thickness, L.
b_i	thickness of layer i ($b_i=\Delta z_i$), L.
B	flow boundary.
B^e	element boundary.
$[B]^e$	mass matrix.
c	concentration of dissolved constituent, ML^{-3}.
$\hat{c}$	trial function.
c_{Jj}	value of concentration at node J in sublayer j, ML^{-3}.
c_p	concentration in the discharging well, ML^{-3}.
D_0	coefficient of molecular diffusion, L^2T^{-1}.
D_L	coefficient of longitudinal dispersion, L^2T^{-1}.
D_T	coefficient of transverse dispersion, L^2T^{-1}.
D_{xx}, D_{yy}, D_{xy}	components of hydrodynamic dispersion tensor in Cartesian coordinates, L^2T^{-1}.
D_s, D_n, D_z	components of hydrodynamic dispersion tensor in curvilinear coordinates, L^2T^{-1}.
$[E]^e$	element coefficient matrix.
$[E_D]^e$	element matrix associated with dispersive terms.
$[E_v]^e$	element matrix associated with advective terms.
$[E^s]$	component of global coefficient matrix in s direction.
$[E^n]$	component of global coefficient matrix in n direction.
$[F_I]^e$	element right-hand side vector.
h	hydraulic head, L.
h_1, h_2, h_3	scale factors of curvilinear coordinate system.
i, j	sublayer indices.
I, J	nodal indices.
k	time step index.
K	hydraulic conductivity, LT^{-1}.
$[L]$	tridiagonal coefficient matrix.
l, m	dimensions of element, L.
$[M]^e$	influence coefficient mass matrix.
n	coordinate normal to streamline, L.
n'	number of nodal sublayers.
n^*	number of nodes in each nodal sublayer.
n_ψ	number of streamlines in the upper half of the flow plane.
N_J	two-dimensional linear basis functions for node J.
Q	total flow rate of well, L^3T^{-1}.
Q_i	flow rate distributed to the well node in layer i, L^3T^{-1}.
R	solution domain.
R^e	element subdomain.
s	coordinate along a streamline, L.
t	elapsed time, T.
t_D	dimensionless time.
V	magnitude of the Darcy velocity, LT^{-1}.
V_x, V_y	component of Darcy velocity (Cartesian coordinate system), LT^{-1}.
W_I	asymmetric weighting function for node I.
x, y	Cartesian coordinates in the flow plane, L.
x_0	one-half well spacing of doublet, L.
z	vertical coordinate, L.
α	upstream parameter.
α^*	maximum allowable value of α.
α_e	calculated value of α for element e.
α_L	longitudinal dispersivity, L.
α_T	transverse dispersivity, L.

α_z vertical dispersivity, L.
v_x, v_n components of unit vector normal to flow boundary.
η_j one-dimensional linear basis function for nodal sublayer j.
ω time weighting factor.
Φ velocity potential function, $L^2\ T^{-1}$.
ψ stream function, $L^2\ T^{-1}$.
θ effective porosity.
ξ^1, ξ^2, ξ^3 generalized orthogonal curvilinear coordinates.

Acknowledgments. This work was supported, in part, by research funds provided to GeoTrans, Inc. and Auburn University by the U. S. Environmental Protection Agency through the Robert S. Kerr Environmental Research Laboratory under assistance agreement CR 810704-01-0 to Auburn University. Although the information described in this article has been funded wholly or in part by the U.S. Environmental Protection Agency, it has not been subjected to the Agency's required peer and administrative review and therefore does not necessarily reflect the views of the Agency and no official endorsement should be inferred. The authors acknowledge Mark Reeves for helpful suggestions in the formulation of equations in curvilinear coordinates.

REFERENCES

Bachmat, Y., and J. Bear, The general equations of hydrodynamic dispersion in homogeneous, isotropic porous mediums, *J. Geophys. Res.*, *69*, 2561–2564, 1964.

Bear, J., *Hydraulics of Groundwater*, McGraw-Hill, 569 pp., New York, 1979.

Brenner, H., The diffusion model of longitudinal mixing in beds of finite length: Numerical values, *Chem. Eng. Sci.*, *17*, 229–243, 1962.

Claassen, H. C., and E. H. Cordes, Two-well recirculating tracer test in fractured carbonate rock, Nevada, *Hydro. Sci. Bull.*, *203*, 367–382, 1975.

Da Costa, J. A., and R. R. Bennett, The pattern of flow in the vicinity of a recharging and discharging pair of wells in an aquifer having areal parallel flow, *Int. Assoc. Sci. Hydrol. Gen. Assem. Berkeley, Publ. 52*, 524–536, 1960.

Douglas, J., Alternating direction methods for three space variables, *Numer. Math.*, *4*, 41–63, 1962.

Douglas, J., and H. H. Rachford, On the numerical solution heat conduction problems in two and three space variables, *Trans. Am. Math. Soc.*, *82*, 421–439, 1956.

Gelhar, L. W., Analysis of two-well tracer tests with a pulse input, *Rep. RHO-BW-CR-131P*, 54 pp., Rockwell Handford Operations, Richlands, Wash., 1982.

Grove, D. B., U.S. Geological Survey tracer study, Armargosa Desert, Nye County, Nevada, II, An analysis of the flow field of a discharging-recharging pair of wells, *U.S. Geol. Surv. Rep. USGS-474-99*, 56 pp., 1971.

Grove, D. B., and W. A. Beetem, Porosity and dispersion constant calculations for a fractured carbonate aquifer using a two-well tracer method, *Water Resour. Res.*, *7*, 128–134, 1971.

Güven, O., R. W. Falta, F. J. Molz, and J. G. Melville, Analysis and interpretation of single-well tracer tests in stratified aquifers, *Water Resour. Res.*, *21*, 676–684, 1985.

Güven, O., R. W. Falta, F. J. Molz, and J. G. Melville, A simplified analysis of two-well tracer tests in stratified aquifers, *Ground Water*, *24*, 1, 1986.

Hassan, Y. A., J. G. Rice, and J. H. Kim, A stable mass-flow-weighted two-dimensional skew upwind scheme, *Numer. Heat Transfer*, *4*, 1–14, 1983.

Hoopes, J. A., and D. R. F. Harleman, Waste water recharge and dispersion in porous media, *J. Hydraulics Div. Am. Soc. Civ. Eng.*, *93*, 51–71, 1967*a*.

Hoopes, J. A., and D. R. F. Harleman, Dispersion in radial flow from a recharging well, *J. Geophys. Res.*, *72*, 3595–3607, 1967*b*.

Huyakorn, P. S., and K. Nilkuha, Solution of transient transport equation using an upstream finite element scheme, *Appl. Math. Model.*, *3*, 7–17, 1979.

Huyakorn, P. S., and G. F. Pinder, *Computational Methods in Subsurface Flow*, 473 pp., Academic, Orlando, Fla., 1983.

Huyakorn, P. S., J. W. Mercer, and D. S. Ward, Finite element matrix and mass balance computational schemes for transport in variably-saturated porous media, *Water Resour. Res.*, *21*, 346–358, 1985.

Huyakorn, P. S., P. F. Anderson, F. J. Molz, O. Güven, and J. G. Melville, Simulations of two-well tracer tests in stratified aquifers at the Chalk River and Mobile Sites, *Water Resour. Res.*, *22*, in press, 1986.

Huyakorn, P. S., B. G. Jones, and P. F. Andersen, Finite element algorithms for simulating three-dimensional groundwater flow and solute transport in multilayer systems, *Water Resour. Res.*, *22*(3), 361–374, 1986*b*.

Jeppson, R. W., Seepage from ditches—Solution by finite differences, *J. Hydraul. Div. Am. Soc. Civ. Eng.*, *94*, 259–284, 1968*a*.

Jeppson, R. W., Axisymmetric seepage through homogeneous and nonhomogeneous porous mediums, *Water Resour. Res.*, *4*, 1277–1288, 1968*b*.

Lapidus, L., and G. F. Pinder, *Numerical Solution of Partial Differential Equations in Science and Engineering*, 677 pp., John Wiley, New York, 1981.

Muskat, M., *Flow of Homogeneous Fluids through Porous Media*, 763 pp., McGraw-Hill, New York, 1937.

Pickens, J. F., and G. E. Grisak, Scale-dependent dispersion in a stratified granular aquifer, *Water Resour. Res.*, *17*, 1191–1211, 1981.

Rosen, M. C., A streamline-upwind finite element method for convection-dominated flows, technical report, Dep. of Mech. and Aerospace Eng., Univ. of Va., Charlottesville, June 1982.

Webster, D. S., J. F. Proctor, and I. W. Marine, Two-well tracer test in fractured crystalline rock, *U.S. Geol. Surv. Water Supply Pap.*, *1544-I*, 22 pp., 1970.

P. F. Andersen, GeoTrans, Inc., 209 Elden Street, Suite 301, Herndon, VA 22070.

O. Güven, Department of Civil Engineering, Auburn University, Auburn, AL 36849.

P. S. Huyakorn, GeoTrans, Inc., 209 Elden Street, Suite 301, Herndon, VA 22070.

F. J. Molz, Department of Civil Engineering, Auburn University, Auburn, AL 36849.

(Received April 19, 1985;
revised December 20, 1985;
accepted January 22, 1986.)

NOTICE

This document has been reviewed in accordance with U.S. Environmental Protection Agency policy and approved for publication. Mention of trade names or commercial products does not constitute endorsement or recommendation for use.

This article documents research that was conducted under the auspices of the U.S. Environmental Protection Agency (USEPA). As an arm of the government, the USEPA has a paid up, non-exclusive, irrevocable, worldwide license to reproduce, prepare derivative works, and distribute to the public all of the material contained herein, and to grant others acting on its behalf the right to do so. The USEPA grants to the National Technical Information Service, Department of Commerce, the right to act as its agent in the distribution of this material.